J Appl Electrochem (2009) 39:737–745
DOI 10.1007/s10800-008-9718-9

ORIGINAL PAPER

# Effect of alternating voltage passivation on the corrosion resistance of duplex stainless steel

**Huan He · Tao Zhang · Chengzhi Zhao · Kai Hou · Guozhe Meng · Yawei Shao · Fuhui Wang**

Received: 14 May 2008 / Accepted: 5 November 2008 / Published online: 29 November 2008


**Abstract** Potentiodynamic polarization and $E_{corr}$ versus $t$ curves were obtained, together with electrochemical impedance spectroscopy (EIS) measurements, in order to understand the effects of alternating voltage (AV) passivation on the corrosion resistance of duplex stainless steel (DSS). SEM, EDS and XPS were employed to further investigate the influence of AV passivation on the properties of the passive film. The results of the electrochemical measurements showed that AV passivation significantly improved the corrosion resistance of DSS. SEM images indicated that the surface exhibited a unique morphology after AV passivation treatment, and XPS results suggested that AV passivation greatly increased the thickness of the passive film. Furthermore, significant chromium enrichment and a higher ratio of $Fe^{3+}/Fe^{2+}$ were observed in the passive film after AV passivation. Mott–Schottky results confirmed that AV passivation had a strong influence on the semiconducting properties of the passive film.

**Keywords** Duplex stainless steel · Alternating voltage passivation · Passive film · Corrosion · XPS analysis

H. He · T. Zhang (✉) · C. Zhao · K. Hou · G. Meng · Y. Shao · F. Wang
Corrosion and Protection Laboratory, College of Material Science and Chemical Engineering, Harbin Engineering University, Nantong ST 145, Harbin 150001, China
e-mail: zhangtao@hrbeu.edu.cn

T. Zhang · G. Meng · Y. Shao · F. Wang
State Key Laboratory for Corrosion and Protection, Institute of Metal Research, Chinese Academy of Sciences, Wencui RD 62, Shenyang 110016, China

## 1 Introduction

Duplex stainless steels are a relatively new class in the stainless steels family. They are comprised of virtually equal amounts of face-centered-cubic austenitic (fcc, $\gamma$-phase) and body-centered-cubic ferritic (bcc, $\alpha$-phase) structures. They combine the attractive properties of austenitic and ferritic stainless steels: high tensile strength and fatigue strength, good toughness even at low temperatures, adequate formability and weldability and excellent resistance to stress corrosion cracking, pitting and general corrosion [1, 2]. Therefore, DSS becomes a replacement for austenitic stainless steels in aggressive environments, and their performance has become an important topic for material scientists and process chemical engineers.

The improvement of corrosion resistance is a key purpose in the development of new stainless steels [3]. It is well known that the resistance of metals/alloys to localized corrosion is related to the quality of their passive films, i.e. their chemical composition, structure and thickness [4, 5]. Various surface treatment techniques including ion implantation and laser treatment have been made to enhance their corrosion resistance [6, 7], but the high costs and rather small treatment-areas limit their applications.

Alternating voltage (AV) passivation is an environmentally-friendly surface technology which is attractive for industrial applications because it can be carried out at a lower temperature and uses a bath without $Cr^{6+}$ ions. It greatly improves the corrosion resistance of austenitic stainless steels in some corrosive media [8–10], but has not been applied to duplex stainless steels. Therefore the purpose of the present investigation was to use it on duplex stainless steel and investigate its effect on the corrosion resistance, and on the morphology, chemical structure and electronic structure of the passive film thus formed.

## 2 Experimental procedures

### 2.1 Materials and samples

ASTM A890 Grade 3A duplex stainless steel was used in this study, with the chemical composition (in wt.%) as follows: 25.6 Cr, 5.37 Ni, 2.4 Mo, 0.23 N, 0.028 C, 0.36 Mn, 0.45 Si, 0.027 P, 0.007 S, Fe (balance). It was cast in a vacuum induction furnace as a cylinder with length 250 mm and diameter 25 mm. Solution annealing was performed in air at 1,100 °C for 60 min, followed by quenching in water. X-ray diffraction analysis (Fig. 1), showed that only ferrite and austenite were present. Specimens sized 10 × 10 × 10 mm were mounted in epoxy resin with an exposed area of 1 $cm^2$, ground to 2,000 grit, polished with 1 μm alumina, degreased in acetone, rinsed with distilled water and dried in air at room temperature.

### 2.2 Passivation

The AV passivation was carried out in 0.5 mol $L^{-1}$ $Na_2SO_4$ aqueous solution at a constant temperature of 20 °C. The amplitude of the square wave was 1,920 mV resulting in potentials of +980 and −940 mV (SCE) as upper and lower limits, respectively. The pulse width was 33 ms and the ratio of the anodic to cathodic time was 7/3. The total passivation time was 30 min. Figure 2, which shows the polarization curve and the applied potential square wave, gives a schematic illustration of the experimental approach. For comparison, DC passivation was carried out at +20 mV (SCE) for the same length of time. All the passivation experiments were carried out on a Zahner IM6ex potentiostat.

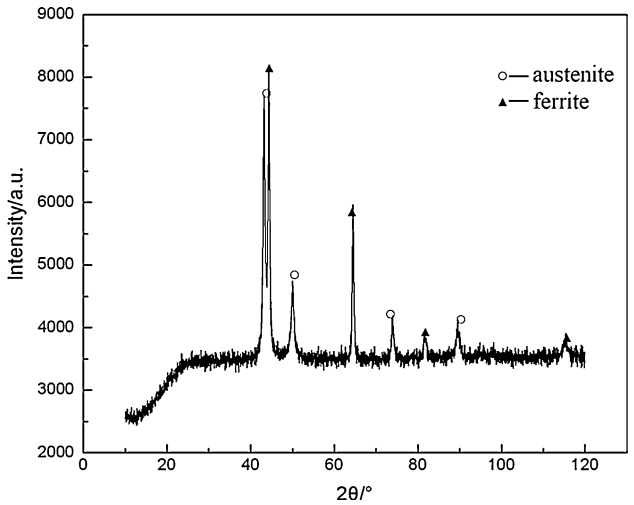


**Fig. 1** Diffractogram of the ASTM A890 Grade 3A DSS after solution annealing at 1,100 °C and water quenching

### 2.3 Electrochemical measurements

Electrochemical methods were used to characterize the corrosion resistance of the as-received, DC- and AV-passivated samples. For all experiments, a three-electrode cell was used with a standard calomel electrode (SCE) as a reference electrode and a platinum counter electrode (20 × 20 mm). All experiments were carried out at a constant temperature of approximately 20 °C. For better reproducibility, all the experiments were repeated more than three times. They were performed on a Zahner IM6ex potentiostat controlled by a PC, which was also used for the acquisition, storage and plotting of data.

Potentiodynamic polarization experiments were carried out in a solution of 0.4 mol $L^{-1}$ NaCl + 0.25 mol $L^{-1}$ $H_2SO_4$. The scan rate was 0.166 mV $s^{-1}$ and the starting potential was −0.3 V versus open-circuit potential. The experiment was terminated when the current exceeded 1 mA.

The $E_{corr}$ versus $t$ experiments were carried out in a solution of 15% $H_2SO_4$ + 5% HCl in order to determine the stability of the passive films. A model 273 EG&G potentiostat/galvanostat was used, controlled by M352 software provided by EG&G PAR company.

Electrochemical impedance spectroscopy (EIS) was also used to study the corrosion behavior of the passive film. The frequency ranged from 100 kHz to 10 mHz and the perturbing AC amplitude was 5 mV. The measurements were carried out on a Zahner IM6ex potentiostat in 0.4 mol $L^{-1}$ NaCl + 0.25 mol $L^{-1}$ $H_2SO_4$ solution.

For the measurement of the Mott–Schottky relationship, a 5 mV sine wave modulated signal, with a frequency of 1 kHz and a step rate of 20 mV $min^{-1}$ was employed.

### 2.4 SEM and EDS analysis

The morphology and composition of the passive film were studied by means of an ACHI S-4700 SEM with an energy dispersive spectrometer (EDS).

### 2.5 XPS analysis

X-ray photoelectron spectroscopy (XPS) analysis was performed on a PHI 5700 ESCA spectrometer with an Al Kα (1486.6 eV) X-ray source operated at 13 kV and 300 W. Depth profiling was achieved by argon ion bombardment with ion energy of 3 keV. The sputtering rate was about 3 nm $min^{-1}$ for $SiO_2$. The measured sample current during depth profiling was 1 μA, and the bombardment area was 4 × 4 mm. The core-level spectra for films were obtained at take-off angles of 45°. Ion sputtering was performed at a pressure of $10^{-7}$ Pa using high-purity argon. Peak identification was performed by reference to an

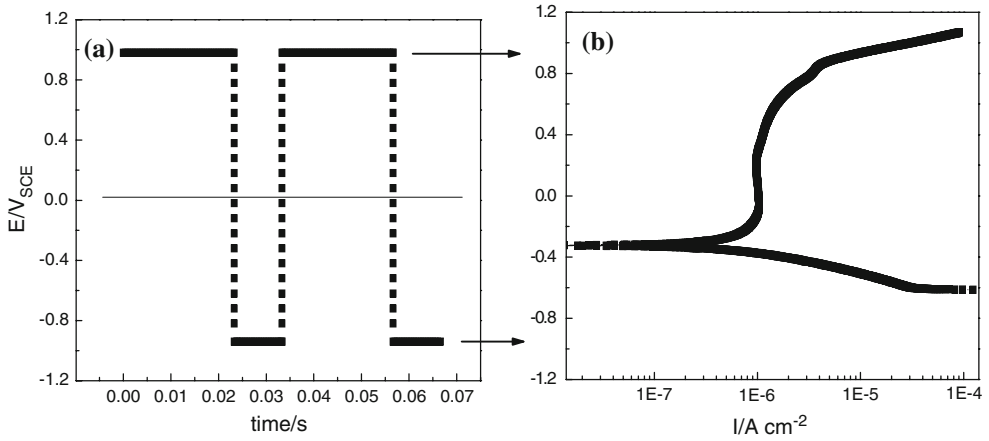


**Fig. 2** Schematic illustration of the measurement principle (**a**) locations of the square wave in comparison with polarization curve, (**b**) polarization curve in the passivation solution of 0.5 mol/L $Na_2SO_4$

XPS database. The binding energy was corrected for charging effects by referencing to the Cls peak.

## 3 Results and discussion

### 3.1 Effect of AV passivation on the corrosion resistance of duplex stainless steel

#### *3.1.1 Potentiodynamic polarization curves*

Potentiodynamic polarization curves for three samples in 0.4 mol $L^{-1}$ NaCl + 0.25 mol $L^{-1}$ $H_2SO_4$ solution are shown in Fig. 3. The breakdown potentials ($E_b$) of the three samples were similar. After AV passivation treatment, the corrosion potential ($E_{corr}$) was found to shift about 250 mV towards the noble direction, and the passive current density was one order of magnitude lower than those of the DC-passivated and the untreated samples. For stainless steels, the passive current density is a very important parameter because it is a measure of the corrosion resistance of the material in the passive state. A lower passive current density indicated a higher corrosion resistance of the material in this environment.

#### *3.1.2 $E_{corr}$ versus t curves*

A comparison of the stability of the surface layers in an acidic solution of 15% $H_2SO_4$ + 5% HCl was obtained from the potential decay curves, which are shown in Fig. 4. It indicates that the stability of the passive film was improved by the AV passivation treatment. The untreated sample and the DC passivation sample reached the active state almost immediately after exposure in the acid solution. The passive film produced by AV passivation underwent gradual degradation.

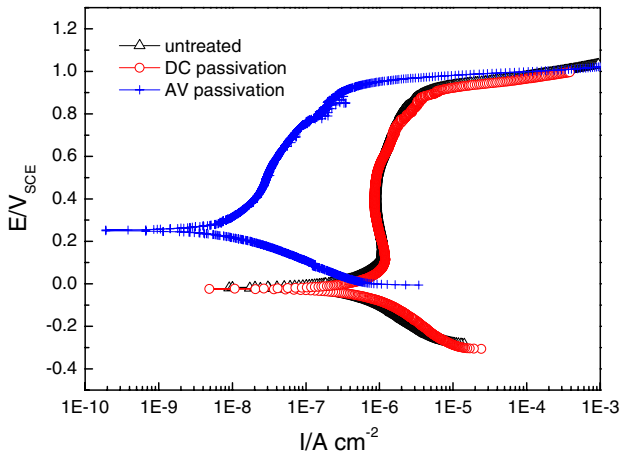


**Fig. 3** Potentiodynamic polarization curves in 0.4 mol/L NaCl + 0.25 mol/L $H_2SO_4$

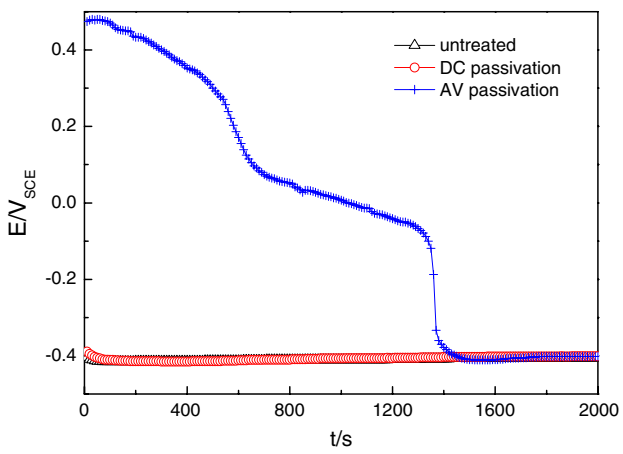


**Fig. 4** Open-circuit potential decay in 15% $H_2SO_4$ and 5% HCl

### 3.1.3 EIS

EIS measurements were performed to investigate the corrosion behavior of the samples in 0.4 mol $L^{-1}$ NaCl + 0.25 mol $L^{-1}$ $H_2SO_4$ solution. The Bode and Nyquist plots are shown in Fig. 5. For all three samples, the EIS plots consisted of two capacitive loops in the high and low frequency range. Those in the high frequency range are associated with the charge transfer at the interface, while those in the low frequency range are associated with the passive film formed on the alloy surface [11].

The equivalent circuit in Fig. 6 is proposed to fit the EIS data. The parallel-connected elements ($R_{film}$, $CPE_{film}$) were used to represent the information of the passive layer on the metal surface. $R_{ct}$ and $CPE_{dl}$ could be attributed to the charge transfer process in which $R_{ct}$ was the charge transfer resistance, and $CPE_{dl}$ represented the double layer capacitance.

The impedance parameters for the tested samples were computed and are summarized in Table 1. The enormous increase in $R_{film}$ means that the corrosion resistance of DSS was improved significantly by the AV passivation treatment. The decrease in $CPE_{film}$ indicates that there was a dense passive film formed on the DSS surface by AV passivation.

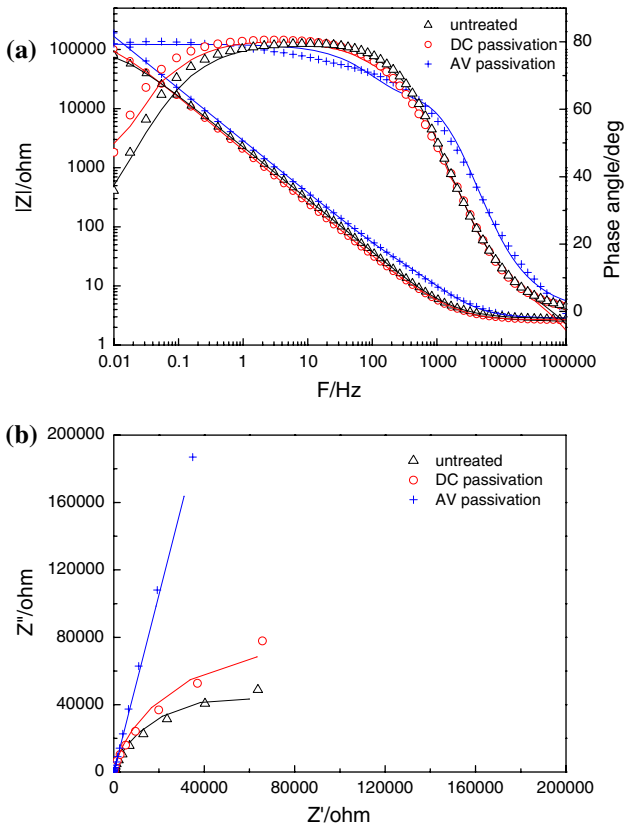


**Fig. 5** EIS plots of three kinds of specimens in 0.4 mol/L NaCl + 0.25 mol/L $H_2SO_4$. **a** Bode plots, **b** Nyquist plots

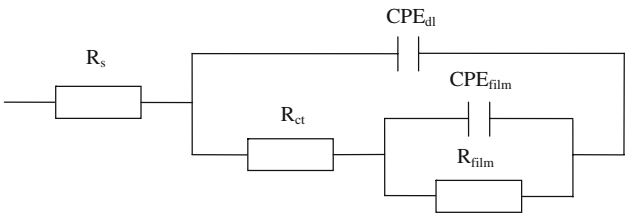


**Fig. 6** Equivalent circuit proposed to fit the experimental EIS data

These results indicate that the AV passivation treatment creates a superior passive film and significantly improves the corrosion resistance of duplex stainless steel.

## 3.2 Effect of AV passivation on the properties of passive film

### 3.2.1 Effect of AV passivation on the surface morphology of passive film

Figure 7 shows the surface morphology of the treated and untreated samples. The surface morphology after AV passivation was unique, and the features on each phase were clearly different.

It is frequently reported that the main alloying elements, i.e. chromium, molybdenum, nickel and nitrogen, are not evenly distributed in the ferrite and austenite of DSS. Chromium and molybdenum are enriched in the ferrite, whereas nickel and nitrogen are concentrated in the austenite [12, 13]. The EDS analysis results (Fig. 8), which are listed in Table 2, indicate that the dark phase was ferrite (characterized by higher Cr and lower Ni content) and the light phase was austenite (distinguished by higher Ni and lower Cr content).

### 3.2.2 Effect of AV passivation on the chemical structure of passive film

All of the above results demonstrated that the AV passivation treatment had a significant influence on the corrosion resistance of duplex stainless steel. In order to understand this effect, the chemical structure of the passive films was analysed by means of XPS.

Figure 9 shows the depth concentration profiles of the passive films. The thickness was determined as the depth at which the composition of the passive film tended to be constant [10]. As shown in Fig. 9, the thickness of the passive film after AV passivation was about 2,100 nm, which was about 60 times thicker than DC-passivated (45 nm) and untreated samples (36 nm). The great increase of the thickness of the passive film by AV passivation would improve the corrosion resistance of the passive film in aggressive media.

**Table 1** Equivalent circuit parameters

| | $R_s$ ($\Omega$ cm$^2$) | $CPE_{dl}$ ($\mu$F cm$^{-2}$) | $R_{ct}$ ($\Omega$ cm$^2$) | $CPE_{film}$ ($\mu$F cm$^{-2}$) | $R_{film}$ (K$\Omega$ cm$^2$) |
|---|---|---|---|---|---|
| Untreated | 2.9 ± 0.1 | 29.88 ± 1.49 | 4.35 ± 0.21 | 59.43 ± 2.93 | 109.00 ± 5.30 |
| DC-passivated | 2.7 ± 0.2 | 60.56 ± 3.02 | 17.15 ± 0.84 | 35.13 ± 1.76 | 167.00 ± 7.37 |
| AV-passivated | 2.8 ± 0.2 | 50.09 ± 2.54 | 94.77 ± 0.47 | 18.57 ± 1.84 | 538.5E5 ± 28.1 E5 |

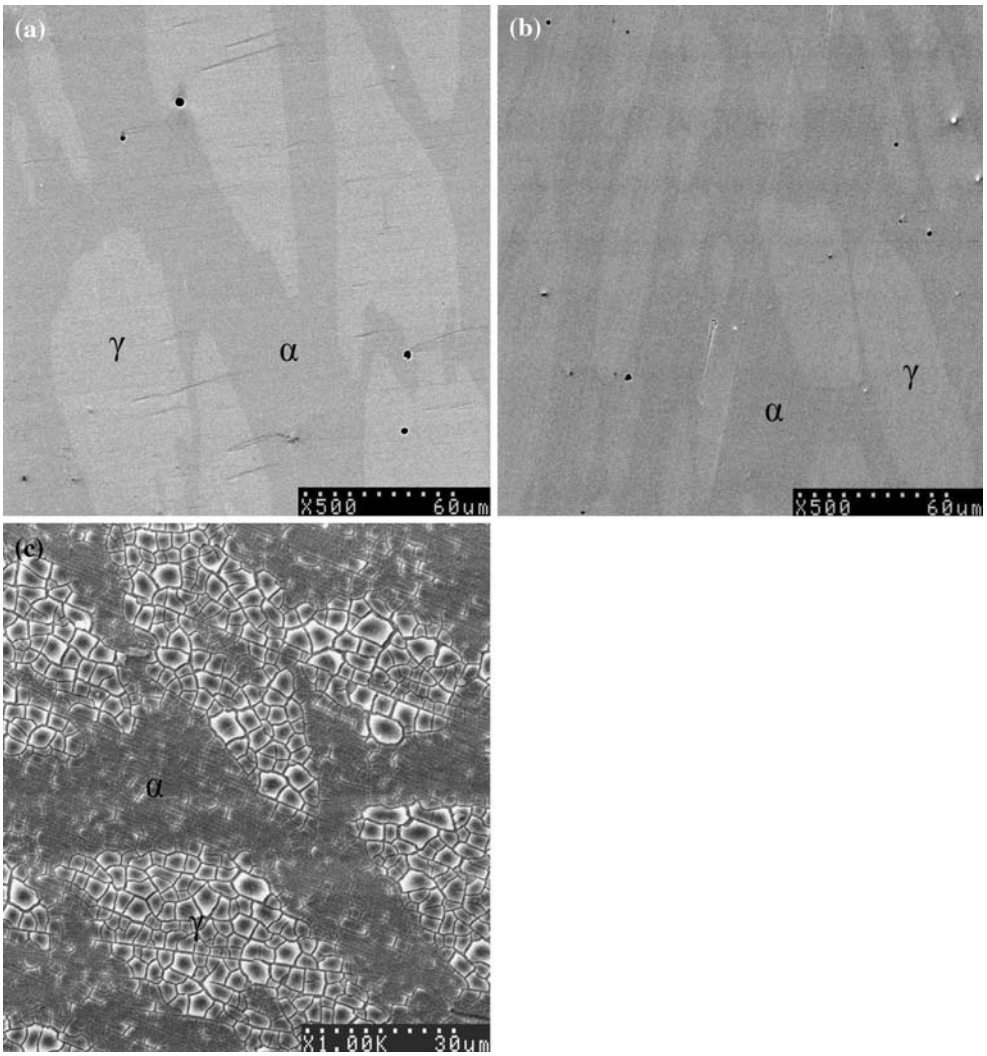


**Fig. 7** SEM photomicrograph of the surface morphology. **a** Untreated, **b** DC-passivated, **c** AV-passivated

It was obvious that there was significant chromium enrichment in the AV passive film with respect to the untreated and DC-passivated samples. Figures 10 and 11 show that there was a much higher atomic Cr/(Cr + Fe) ratio and lower Fe elemental concentration in the AV-passivated film compared with the DC-passivated and untreated ones. The strong chromium enrichment in the film can be explained by the preferential dissolution of Fe ions into the electrolyte [14].This high chromium enrichment must play a very important role in the improvement on the corrosion resistance of DSS after AV passivation.

The fitted XPS spectra were obtained to determine the chemical state of Fe of the passive films. Figure 12 indicated that the ratio of $Fe^{3+}/Fe^{2+}$ in the passive film after AV passivation was much higher than in the DC-passivated and untreated ones. For the reason that $Fe^{3+}$ is more stable than $Fe^{2+}$, the passive film after AV passivation would be more stable.

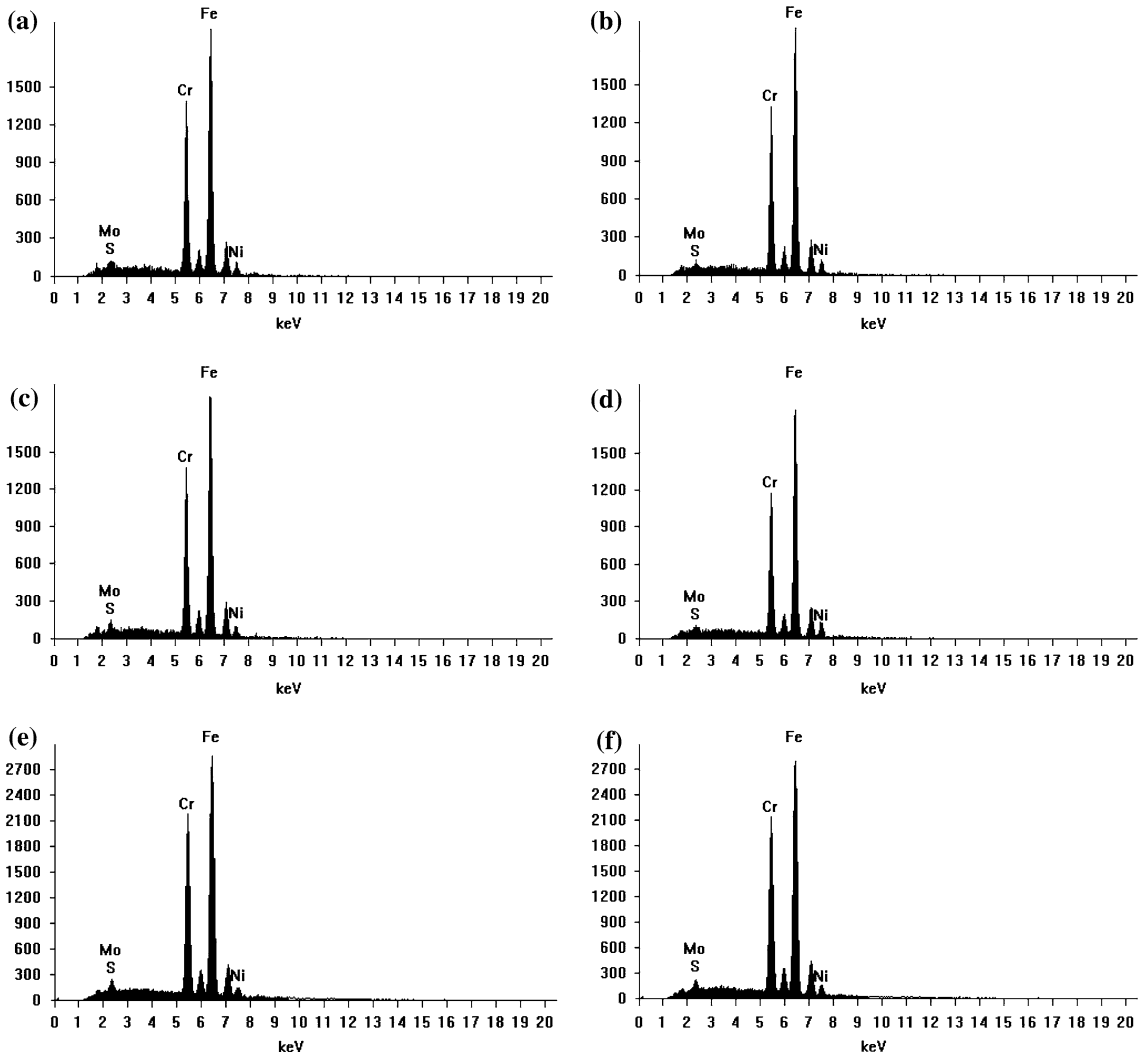


**Fig. 8** EDS spectra of the samples. **a** Dark phase of the untreated sample, **b** light phase of the untreated sample, **c** dark phase of the sample after DC passivation, **d** light phase of the sample after DC passivation, **e** dark phase of the sample after AV passivation, **f** light phase of the sample after AV passivation

**Table 2** EDS results of chemical composition (wt.%)

| | Untreated (α) | Untreated (γ) | DC (α) | DC (γ) | AV (α) | AV (γ) |
|---|---|---|---|---|---|---|
| Cr | 25.482 | 24.379 | 25.393 | 23.693 | 27.993 | 26.873 |
| Ni | 5.346 | 7.461 | 5.563 | 8.004 | 4.223 | 5.715 |

Fitted XPS spectra were obtained to determine the chemical state of Fe in the passive films. Figure 12 indicates that the ratio of $Fe^{3+}/Fe^{2+}$ in the passive film after AV passivation was much higher than in the DC-passivated and untreated ones. $Fe^{3+}$ is more stable than $Fe^{2+}$, therefore the passive film after AV passivation would be more stable.

In brief, the effects of AV passivation treatment can be summarized in terms of three aspects: a significant increase of the passive film thickness, great enrichment of chromium and an increase in the ratio of $Fe^{3+}/Fe^{2+}$ in the passive film.

### 3.2.3 *Effect of AV passivation on the electronic structure of passive film*

It is well known that there are relationships between the semiconducting properties and the corrosion resistance of a passive film. These properties can be determined by analyzing the curves of capacitance as a function of the electrode potential, which reflects the charge distribution in the passive films. The charge distribution at the interface of a semiconductor and an electrolyte is always determined by measuring the capacitance of the space charge layer (*C*sc) as a function of the electrode potential (*E*). The interfacial capacitance, *C*, is obtained from $C = -1/\omega Z''$. Assuming that the capacitance of the Helmholtz layer can be

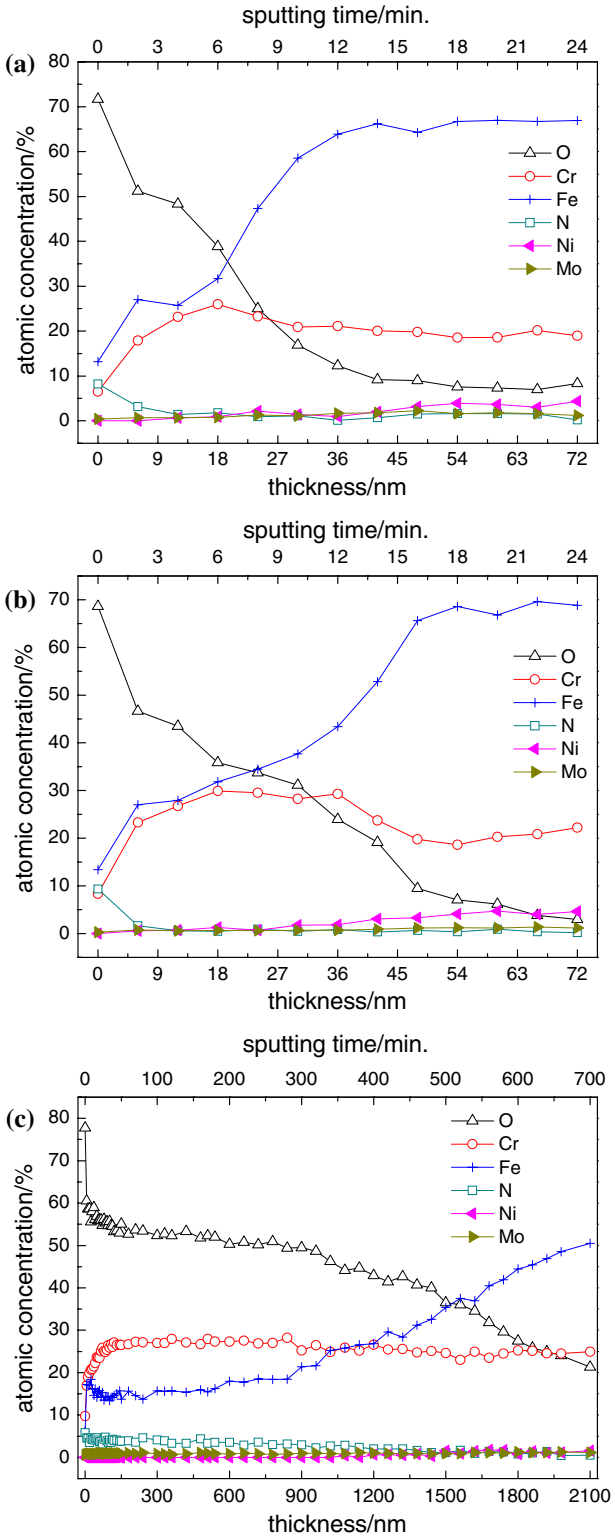


**Fig. 9** Depth composition profiles of the passive films on DSS. **a** Untreated, **b** DC-passivated, **c** AV-passivated

neglected, the measured capacitance $C$ is equal to the 'space charge' capacitance, $C$sc [15]. According to the Mott–Schottky theory [16, 17], the space charge

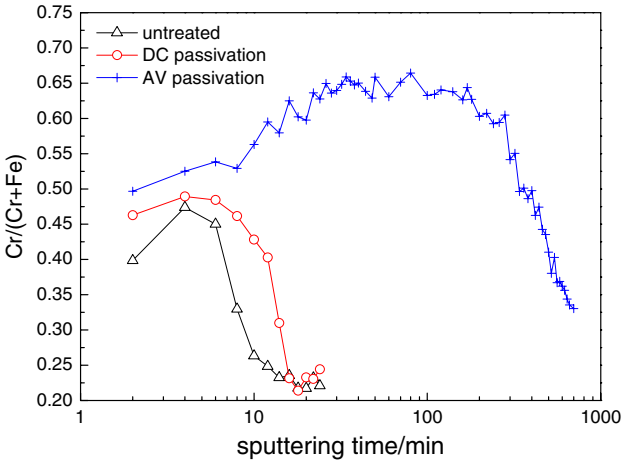


**Fig. 10** Profiles of Cr/(Cr + Fe) in the passive films

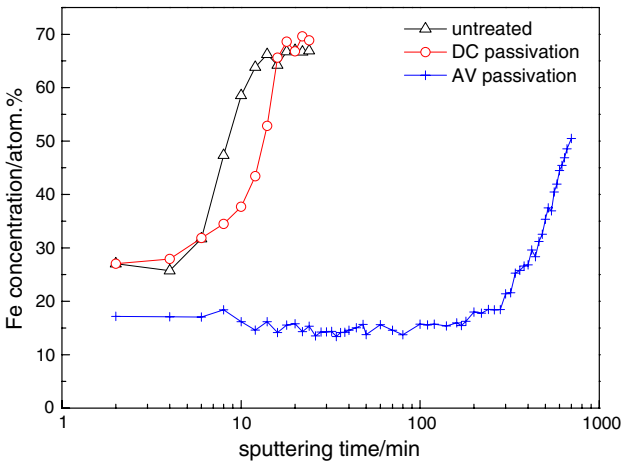


**Fig. 11** Profiles of Fe in the passive films

capacitance of an n-type and a p-type semi-conductor are given by Eqs. 1 and 2, respectively.

$$\frac{1}{C^2} = \frac{2}{\varepsilon\varepsilon_0 e N_D}\left(E - E_{FB} - \frac{KT}{e}\right) \quad (1)$$

$$\frac{1}{C^2} = -\frac{2}{\varepsilon\varepsilon_0 e N_A}\left(E - E_{FB} - \frac{KT}{e}\right) \quad (2)$$

where $\varepsilon$ is the dielectric constant of the passive film, $\varepsilon_0$ is the permittivity of free space ($8.854 \times 10^{-14}$ F/cm), $e$ is the electron charge ($1.602 \times 10^{-19}$ C), $K$ is the Boltzmann constant ($1.38 \times 10^{-23}$ J/K), $T$ is the absolute temperature and $KT/e$ is approximately 25 mV at room temperature, $E_{FB}$ is the flat band potential which can be obtained from the extrapolation of $1/C^2$ to 0, $N_D$ and $N_A$ are the donor and acceptor densities that can be determined from the slope of the experimental $1/C^2$ versus applied potential ($E$) assuming the dielectric constant of the passive film $\varepsilon$ on the stainless steels as 15.6 [18].

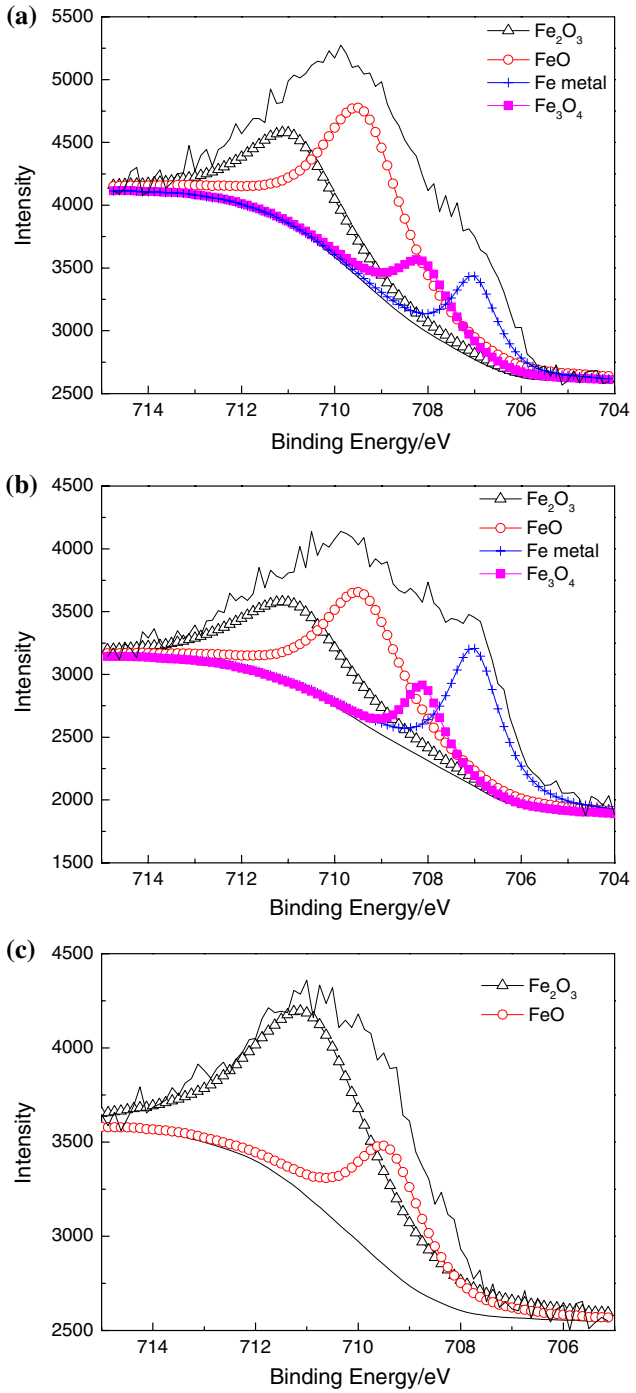


**Fig. 12** Examples of fitted Fe $2p_{3/2}$ XPS spectra by $Ar^+$ sputtering for 2 min. **a** Untreated, **b** DC-passivated, **c** AV-passivated

The Mott–Schottky plots in 0.4 mol $L^{-1}$ NaCl + 0.25 mol $L^{-1}$ $H_2SO_4$ solution are shown in Fig. 13. Depending on the applied potential, two linear regions are apparent in all these plots with a positive and negative slope characterized by different capacitance behavior. The positive region of the straight line indicates n-type semiconducting behavior. In the second potential region, the negative potential region of the straight line indicates p-type semiconducting behavior of the passive film. It can be seen that both the n-type and p-type semiconductivity were strongly affected by AV passivation. The influence of the passivation treatments on DSS on the slopes and the values of the donor and acceptor densities are shown in Table 3. It is observed that both the donor and acceptor densities decreased after AV passivation. Lower donor and acceptor concentration implies an improvement of the corrosion resistance.

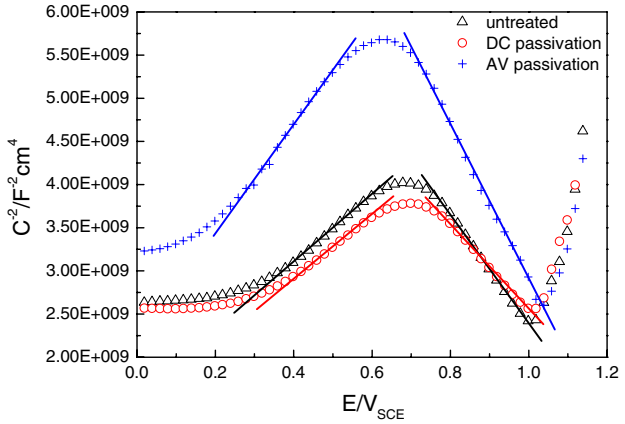


**Fig. 13** Mott–Schottky plots in 0.4 mol/L NaCl + 0.25 mol/L $H_2SO_4$

**Table 3** Influence of the passivation treatments on DSS on the values of the slopes, the donor and acceptor densities (respectively, $N_D$ and $N_A$)

| | n-Type semiconductivity | | p-Type semiconductivity | |
|---|---|---|---|---|
| | Slope | $N_D$ ($m^{-3}$) | Slope | $N_A$ ($m^{-3}$) |
| Untreated | 3.927E9 | 23.017E26 | −6.426E9 | 14.066E26 |
| DC-passivated | 3.539E9 | 25.540E26 | −5.056E9 | 17.877E26 |
| AV-passivated | 6.246E9 | 14.471E26 | −9.053E9 | 9.984E26 |

## 4 Conclusions

All the electrochemical experimental results indicated that a significant improvement in the corrosion resistance of duplex stainless steel (DSS) was achieved after AV passivation, which is attributed to the excellent passive film formed on the DSS surface.

AV passivation had a strong influence on both the chemical and electronic structure of the passive film. For the chemical structure, the effect of AV passivation treatment can be summarized in terms of three aspects: a significant increase in the thickness of the passive film,

great enrichment of chromium and an increase in the ratio of $Fe^{3+}/Fe^{2+}$ in the passive film. All the above three aspects were beneficial to the corrosion resistance of DSS.

For the electronic structure, AV passivation treatment decreased the donor and acceptor densities in the passive film, which is an important factor for the enhancement of corrosion resistance.

The success of the alternating voltage passivation of DSS is especially significant in various aggressive environments, which can easily destroy the passive layers on stainless steels. The AV passivation process can create surface layers with an excellent corrosion resistance on DSS which cannot be obtained by other traditional passivation technologies.

**Acknowledgments** The financial support from Harbin Science and Technology Board under the contract No. 2006AA4CG070 and the research fund of Harbin Engineering University No. heuft05015 are gratefully acknowledged.

## References

1. Muthupandi V, Srinivasan P, Seshadri K, Sundaresan S (2003) Mater Sci Eng A358:9
2. Távara S, Chapetti M, Otegui J, Manfredi C (2001) Int J Fatigue 23:619
3. Sedriks A (1986) Corrosion 42:376
4. Olsson C, Landolt D (2003) Electrochim Acta 48:1093
5. Schultze J, Lohrengel M (2000) Electrochim Acta 45:2499
6. Pérez F, Hierro M, Gómez C, Martínez L, Viguri P (2002) Surf Coat Tech 155:250
7. Pan Q, Huang W, Song R, Zhou Y, Zhang G (1998) Surf Coat Tech 102:245
8. Kwiatkowski L, Mansfeld F (1993) J Electrochem Soc 140:L39
9. Mansfeld F, Lin S, Kwiatkowski L (1993) Corros Sci 34:2045
10. Song G, Cao C, Lin H (1993) Corrosion 49:271
11. Muñoz A, Antón J, Guiñón J, Pérez V (2007) Corros Sci 49:3200
12. Cortie M, Potgieter J (1991) Met Trans 22A:2173
13. Vannevik H, Nilsson J, Frodigh J, Kangas P (1996) ISIJ Int 36:807
14. Kircheim R, Heine B, Fishmeister H, Hofmann S, Knote H, Stolz V (1989) Corros Sci 29:899
15. Sikora E, Macdonald D (2002) Electrochim Acta 48:69
16. Goodlet G, Faty S, Cardoso S, Freitas P, Simõse A, Ferreira M, Belo M (2004) Corros Sci 46:1479
17. Carmezim M, Simões A, Montemor M, Belo M (2005) Corros Sci 47:581
18. Simões A, Ferreira M, Rondot B, Belo M (1990) J Electrochem Soc 137:82